Published OnlineFirst April 15, 2014; DOI: 10.1158/1535-7163.MCT-13-1067

Small Molecule Therapeutics

Molecular Cancer Therapeutics

# Dual Targeting of Integrin $\alpha_v\beta_3$ and Matrix Metalloproteinase-2 for Optical Imaging of Tumors and Chemotherapeutic Delivery

Jessica L. Crisp[1], Elamprakash N. Savariar[1], Heather L. Glasgow[1,4], Lesley G. Ellies[2], Michael A. Whitney[1], and Roger Y. Tsien[1,3,5]

## Abstract

Activatable cell-penetrating peptides (ACPP) provide a general strategy for molecular targeting by exploiting the extracellular protease activities associated with disease. Previous work used a matrix metalloproteinase (MMP-2 and 9)-cleavable sequence in the ACPP to target contrast agents for tumor imaging and fluorescence-guided surgery. To improve specificity and sensitivity for MMP-2, an integrin $\alpha_v\beta_3$-binding domain, cyclic-RGD, was covalently linked to the ACPP. This co-targeting strategy relies on the interaction of MMP-2 with integrin $\alpha_v\beta_3$, which are known to associate via the hemopexin domain of MMP-2. In U87MG glioblastoma cells in culture, dual targeting greatly improved ACPP uptake compared with either MMP or integrin $\alpha_v\beta_3$ targeting alone. *In vivo*, dual-targeted ACPP treatment resulted in tumor contrast of $7.8 \pm 1.6$, a 10-fold higher tumor fluorescence compared with the negative control peptide, and increased probe penetration into the core of MDA-MB-231 tumors. This platform also significantly improved efficacy of the chemotherapeutic monomethylauristatin E (MMAE) in both MDA-MB-231 orthotopic human and syngeneic Py230 murine breast tumors. Treatment with cyclic-RGD-PLGC(Me)AG-MMAE-ACPP resulted in complete tumor regression in one quarter of MDA-MB-231 tumor–bearing mice, compared with no survival in the control groups. This rational mechanism for amplified delivery of imaging and potent chemotherapeutic agents avoids the use of antibodies and may be of considerable generality. *Mol Cancer Ther; 13(6); 1514–25. ©2014 AACR.*

## Introduction

Activatable cell-penetrating peptides (ACPP) provide a universal and modular strategy for tissue targeting and molecular imaging of extracellular protease activity *in vivo*. ACPPs consist of a polycationic cell-penetrating peptide (CPP) attached to a polyanionic sequence via a protease-cleavable linker. The polyanion prevents adhesion and uptake of the CPP and its cargo until localized protease activity cleaves the substrate sequence, allowing the inhibitory domain to dissociate (1). The released CPP then binds cells in its immediate proximity and is typically endocytosed. For tumor imaging, the main protease targets have been matrix metalloproteinase (MMP)-2 and -9, which are pivotal in matrix degradation, inflammation, and tumor cell migration, and whose activity is heightened in most invasive cancers (2–4). Although MMP-cleavable ACPPs have successfully been used to visualize tumors with fluorescence and MRI, their specificity and sensitivity for MMP-2 could be improved (5–7).

To optimize substrate–enzyme interactions, nature often includes an exosite-binding domain adjacent to a protease cleavage site, which improves both affinity and specificity for its given enzyme. This study uses a similar strategy to improve ACPP-based tumor targeting. Integrin $\alpha_v\beta_3$ has been shown to bind the hemopexin domain of MMP-2 (8) and is upregulated in many tumors and their vasculature (9–11). Furthermore, integrin $\alpha_v\beta_3$ is reported to be involved in the activation of MMP-2, and the cooperation of the macromolecules could direct localized degradation of the extracellular matrix (12–14). Cyclic-RGD, a popular ligand for integrin $\alpha_v\beta_3$, was added as a co-targeting moiety by attaching it to the inhibitory portion of the ACPP such that protease attack would separate the CPP from the cyclic-RGD-polyglutamate domain. Dissociation of the latter from $\alpha_v\beta_3$ would allow the integrin–MMP complex to bind additional unactivated ACPPs for continued catalytic turnover (Fig. 1).

Dual-targeted radiolabeled tracers that bind integrin $\alpha_v\beta_3$ and are cleaved by MMP-2 have been reported (15). The peptides have only been characterized *in vitro*, but such an approach could be used to investigate the pathophysiology of MMP-2 activity *in vivo* by measuring the

**Authors' Affiliations:** Departments of [1]Pharmacology, [2]Pathology, and [3]Chemistry and Biochemistry, [4]Biomedical Sciences Graduate Program, University of California San Diego, La Jolla, California; and [5]Howard Hughes Medical Institute, Bethesda, Maryland

**Note:** Supplementary data for this article are available at Molecular Cancer Therapeutics Online (http://mct.aacrjournals.org/).

**Corresponding Author:** Roger Y. Tsien, University of California San Diego, 9500 Gilman Drive, La Jolla, CA 92093. Phone: 858-534-4891; Fax: 858-534-5270; E-mail: rtsien@ucsd.edu

**doi:** 10.1158/1535-7163.MCT-13-1067

Published OnlineFirst April 15, 2014; DOI: 10.1158/1535-7163.MCT-13-1067



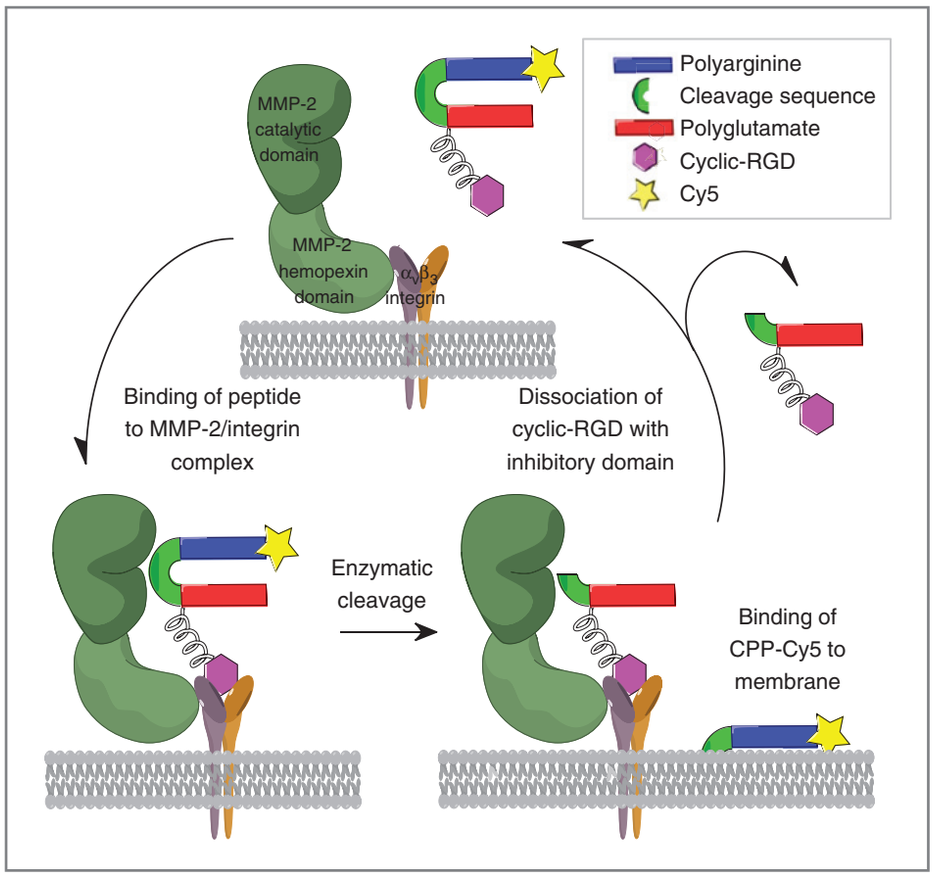


**Figure 1.** Proposed mechanism for dual targeting of integrin $\alpha_v\beta_3$ and MMP-2 with cyclic-RGD-PLGC(Me)AG-ACPP. MMP-2 associates with integrin $\alpha_v\beta_3$ via its hemopexin domain; therefore, it is hypothesized that binding of cyclic-RGD to integrin $\alpha_v\beta_3$ orients the ACPP for proteolysis by the catalytic domain of MMP-2. Once the ACPP is cleaved, the CPP along with its cargo binds to the plasma membrane and gets taken into cancer cells via endocytosis. The cyclic-RGD and polyglutamate domain dissociate from the integrin and allow for continued enzymatic turnover.

ratio of the 2 radioisotopes. Imaging probes have also been developed that combine integrin $\alpha_v\beta_3$ and MMP-2 targeting to detect U87MG glioblastoma subcutaneous tumors (16). Optical contrast ratios of 3.5-fold for tumor compared with adjacent normal tissue were obtained using MMP-dependent dequenching of Cy5.5, although this method provides no mechanism for retaining the probe in tumor. This limits the contrast that can be obtained and hinders potential translation from imaging to therapeutic delivery. ACPPs provide a superior alternative to both these examples because the targeting is a function of CPP activation, which has the advantage of enzymatic amplification, and the polyarginine offers an efficient means of cellular penetration and retention. This amplification and retention should increase tumor uptake compared with the purely stoichiometric association of cyclic-RGD and integrin $\alpha_v\beta_3$.

Monomethylauristatin E (MMAE) is a synthetic analogue of dolistatin-10, a potent inhibitor of microtubule polymerization that was originally isolated from the Indian Ocean sea hare *Dolabella auricularia* (17, 18). Problems with toxicity have limited its effectiveness as an unconjugated drug, but it has found clinical success by linkage to antibodies. The anti-CD30 antibody–auristatin conjugate has been approved for cancer therapy (19), and several others are in various stages of clinical development (20). These achievements suggest that other targeting approaches, including ACPP-based mechanisms, may be useful for expanding the clinical use of MMAE. This report demonstrates that when integrin and MMP targeting strategies are combined, the resulting ACPP has greater uptake into cancer cell lines, enhanced tumor uptake and contrast *in vivo*, and superior penetration into malignant tissue. Furthermore, peptide conjugation with MMAE leads to regression and cures of established primary tumors.

## Materials and Methods

### Peptide synthesis

Co-targeted ACPPs were synthesized by following similar synthetic procedures reported in (21). The therapeutic peptides were made as follows: with "mal" denoting maleimidyl, and "suc" denoting succinimidyl, the reaction product of mal with a free cysteine. $NH_2$-$e_9$-o-PLGC(Me)AG-o-c-$r_9$-c(suc-Cy5) (where o = -NH-$CH_2$-$CH_2$-O-$CH_2$-CO-) was reacted with previously synthesized maleimidopropionyl-Val-Cit-PAB-MMAE (22) to generate $NH_2$-$e_9$-o-PLGC(Me)AG-o-c[suc-$(CH_2)_2$-Val-Cit-PAB-MMAE]-$r_9$-c(suc-Cy5). This peptide was reacted with mal-$peg_{12}$-NHS through the N terminus, isolated, and reacted with 2 molar equivalents of cyclic(RGDfC) (Peptide International) in dimethyl sulfoxide (DMSO) to

Published OnlineFirst April 15, 2014; DOI: 10.1158/1535-7163.MCT-13-1067



get the final compound. The product was purified using high-performance liquid chromatography (HPLC), and the identity was verified using electrospray mass spectrometry. To generate the control peptides, cyclic(RGDfC) was replaced by cyclic(RADfC) and o-PLGC(Me)AG substituted with a PEG6. Detailed chemical synthesis and schemes are provided in Supplementary Data and detailed chemical structures are provided in Supplementary Fig. S1.

### Enzyme cleavage assay

Peptides were diluted to 5 μmol/L in a TRIS buffer (20 mmol/L TRIS, 150 mmol/L NaCl, 2 mmol/L $CaCl_2$, pH 7.5) and placed on ice. The catalytic domain of MMP-2 (Calbiochem) was added (50 nmol/L) and the reaction mixture was transferred to a 37°C incubator. At various time points for up to 4 hours, 10 μL aliquots were removed from the reaction wells, immediately mixed 1:1 with 2× tricine sample buffer (Life Technologies), and heated to 95°C for 60 seconds. Samples were subjected to electrophoresis on 10% to 20% tricine gradient gels (Life Technologies) for 90 minutes at 110 V. Gels where imaged on a Maestro Imager (Perkin Elmer) using an excitation filter of 620/22 nm and an emission filter of 670/20 nm. Using ImageJ, the integrated intensity was measured for the uncleaved and cleaved peptide bands in each lane of the gel, ensuring that the box used to define the region of interest remained constant. The following equation was used to calculate the extent of cleavage: percent cleavage = 100 × [cleaved peptide/(cleaved peptide + uncleaved peptide)]. A plot was generated that graphed percent of cleaved peptide as a function of time.

### Integrin-binding assay

All human cells lines included in this study where purchased from and verified by American Type Culture Collection (ATCC) and used within 6 months of being received or frozen within a few passages from purchase and thawed before experimentation. High protein-binding 96-well plates were coated with vitronectin at a concentration of 10 μg/mL in PBS at 4°C overnight. The plates were rinsed 3 times with Tris-buffered saline (TBS) containing 0.02% Tween, blocked with 2% bovine serum albumin (BSA) in PBS for 1 hour at room temperature (RT), and then rinsed again. MDA-MB-435 cells [ATCC; cultured in Eagle's minimum essential media (EMEM; ATCC) with 10% FBS at 37°C with 5% $CO_2$] were rinsed with PBS and detached by incubating with 0.48 mmol/L $EDTA(Na)_4$ (Versene, Gibco) at RT for 15 to 20 minutes. Cells were resuspended in serum-free media containing Calcein Green AM ester (Life Technologies) at a concentration of $1 \times 10^6$ cells/mL and then peptides were added such that the final concentration ranged from 0 to 10 μmol/L. The cells were incubated at RT for 20 minutes and then transferred to vitronectin-coated plates and incubated an additional 20 minutes to allow attachment. Unbound cells were removed by gently washing 3× with serum-free imaging buffer [Dulbecco's Modified Eagle's Media (DMEM) without phenol red (CellGrow), 20 mmol/L HEPES, GlutaMAX (Gibco)]. Calcein Green fluorescence was measured on a plate reader (Tecan) with 490 nm excitation and 520 nm emission.

### Cellular uptake and confocal imaging

U87MG cells (ATCC) were cultured in DMEM (CellGrow) with 10%FBS, GlutaMAX (Gibco), and 1% penicillin/streptomycin at 37°C with 5% $CO_2$. For imaging, cells were plated on sterile glass bottom 96-wells plates (25,000 cells per well) and allowed to settle overnight. Peptides were diluted to a concentration of 1 μmol/L in serum-free imaging buffer. Culture media were aspirated, and the cells were treated with peptide for 30 minutes at 37°C and then washed 3× before a 100 μL of imaging buffer containing 10% FBS and 20 μg/mL Calcein Blue AM ester (Life Technologies) was added. Imaging was performed on a Zeiss 5-Live line scanning confocal microscope using a 40× water objective with the following settings: 635 nm excitation laser and 650 nm long pass emission filter (Cy5) and a 405 nm excitation laser and 415 to 450 nm emission filter (Calcein Blue).

### Tumor model generation and *in vivo* fluorescence imaging

All animal studies were done in compliance with the principles and procedures outlined by the Institutional Animal Care and Use Committee at the University of California San Diego (La Jolla, CA). MDA-MB-231 cells (ATCC) were cultured in EMEM with 10% FBS at 37°C with 5% $CO_2$ and female athymic *nu/nu* mice, 5 to 6 weeks of age, were purchased from Harland Labs or bred at UCSD by the animal care program (ACP). To generate tumors, $0.5 \times 10^6$ to $1 \times 10^6$ MDA-MB-231 cells were injected into the mammary fat pads of female mice in a vehicle of 4 mg/mL Matrigel with an injection volume of 40 μL. Tumors were allowed to grow until they reached a diameter of 3 to 5 mm. The MMTV-PyMT model in the FVB/N background was used for spontaneous tumor generation (23). For generation of syngeneic cell line tumors, $1 \times 10^6$ Py230 cells originally isolated from a C57Bl/6 spontaneous PyMT tumor (24) were injected into the mammary fat pads of albino C57Bl/6 mice in 10 to 20 μL of 4 mg/mL Matrigel. Tumors grew to 5 to 7 mm diameter in 5 to 6 weeks. The Py230 cells were isolated from a spontaneous MMTV-PyMT tumor in 2004 and have been authenticated by flow cytometry and immunohistochemical staining for mammary cell bipotential markers keratin 8 and keratin 14 as well as luminal progenitor cell marker CD61. Tumors arising from Py230 cells have been sectioned and stained to confirm luminal mammary tumor morphology as recently as February 2014.

For optical imaging, mice were anesthetized with an intraperitoneal (IP) injection of 50 μL of a 1:1 mixture of ketamine (100 mg/mL) and midazolam (5 mg/mL; KM).

Published OnlineFirst April 15, 2014; DOI: 10.1158/1535-7163.MCT-13-1067



Cy5-labeled peptides were injected intravenously via the tail vein at a dose of 10 nanomoles. At 6 hours postinjection, mice were again anesthetized with an IP dose of KM and imaged using the Maestro Small Animal Imager with an excitation filter of 620/22 nm and a 645 nm long-pass emission filter with the dichroic filter tuned to 670 nm.

To generate Py230 lung metastases, $5 \times 10^5$ cells were injected into the tail vein of C57Bl/6 mice and after 4 to 5 weeks, multiple microscopic lung metastases developed. Animals were then injected with 10 nanomoles of cyclic-RGD-PLGC(Me)AG-ACPP and sacrificed 6 hours later. The trachea was exposed and the lungs were inflated with 800 μL PBS, then the trachea was clamped, and the lungs were excised. Whole lungs were imaged on the Maestro using excitation filter of 620/22 nm and an emission filter of 645 nm long-pass with the dichroic filter tuned to 670 nm.

### Tumor contrast ratio calculation

Images of mice with the skin removed were analyzed with Image J. A 30-by-30 pixel box was used to measure the integrated fluorescent density for 10 regions of the tumor and 10 regions of tissue immediately adjacent to the tumor. To determine the background fluorescence, a black slate was imaged at the same exposure time and then the average fluorescent density was measured and subtracted from the tissue values. The values for each animal were averaged, and the contrast ratio was calculated by dividing the tumor fluorescence by the surrounding tissue fluorescence.

### Standardized uptake value calculation

Tumor, liver, kidney, and muscle were harvested, weighed, and placed in 15-mL plastic vials. Standardized uptake value (SUV) buffer (150 mmol/L NaCl, 10 mmol/L TRIS, 2 g/100 mL SDS, 0.25 mg/mL proteinase K, and 0.1 mg/mL DNase, pH 8.0) was added at a ratio of 9 μL buffer per 1 mg tissue. Tissues were homogenized with a point sonicator (Fisher Scientific) using an amplitude range of 5% to 15% for a maximum of 20 seconds. Tissue solutions were placed in a 37°C incubator overnight with constant agitation. About 200 μL was transferred to a well of a black, clear plastic bottom, 96-well plate (Costar) and fluorescence measurements were performed on a plate reader (Tecan) using 630 nm excitation and a 680 nm emission with 12-nm slits. Fluorescent counts were converted to Cy5 concentrations using tissue-specific calibration curves. To calculate the SUV, the peptide concentration in molarity was converted to molality and then normalized by the injected dose and animal weight. The equation for SUV is: SUV = (moles of peptide in tissue/weight of tissue)/(moles of peptide injected/weight of animal).

### Frozen section imaging

Sample tumors from each of the peptide treatment groups were submerged in OCT (Tissue-Tek), snap-frozen in liquid nitrogen, and stored at −80°C. Sections were cut on a cryostat (Leica) at a thickness of 10 μm, then melted directly onto a coverslip, and immediately chilled to −20°C. The tissue remained frozen, whereas images were collected on a 5-Live confocal microscope using a 20× air objective, 635 nm excitation laser, and a 650 nm long-pass emission filter.

### Immunohistochemistry

About 10-μm serial sections of frozen tumor tissue were mounted on to Superfrost slides and fixed with 4% paraformaldehyde (PFA) in PBS for 60 seconds at RT. Sections were washed 3 times in PBS and blocked with 10% normal goat serum (Life Technologies) for 30 to 60 minutes at RT and then the excess serum was aspirated. Primary antibodies for MMP-2 (Abcam, ab37150) and $\alpha_v\beta_3$ (Abbiotec, 251672) were diluted 1:100 in PBS, placed on the tissue, and allowed to incubate overnight at 4°C in the dark within a humidified chamber. Primary antibodies were removed and the sections were washed 3× for 20 minutes each at RT in PBS with slight agitation. Tissue sections were blocked again with goat serum for 20 minutes at room temperature before application of the secondary antibody. Fluorescein isothiocyanate (FITC)-labeled secondary antibody (Santa Cruz, sc-2012) was diluted 1:500 in PBS and incubated for 2 to 3 hours at RT. Sections were washed 3 times for 20 minutes each with PBS and slight agitation and then coverslips were mounted with Prolong Gold (Life Technologies). Imaging was done on the 5-Live microscope using an excitation laser of 488 nm with an emission filter of 500 to 520 nm.

### *Ex vivo* confocal imaging

Mice with MDA-MB-231 mammary tumors were injected with 10 nanomoles cyclic-RGD-PLGC(Me)AG-ACPP and 10 minutes before sacrifice (6 hours after peptide injection), also injected with 250 μg FITC-dextran (10 mg/mL) and 200 μg of Hoechst (10 mg/mL). Tumors were harvested, placed in a glass bottom dish, and imaged using a Zeiss LSM780 point scanning confocal microscope with a 40× water objective.

### Therapeutic peptide imaging *in vitro*

Cal-27 (ATCC), HeLa (ATCC), Panc-1 (ATCC), and PC3 (ATCC) cells were cultured in DMEM with 10% FBS, whereas the MDA-MB-231 (ATCC) and HT1080 (ATCC) cells were grown in EMEM with 10% FBS. Cells were trypsinized and then plated in 96-well glass bottom plates at a density of 20,000 cells per well and allowed to settle for 24 hours. The cyclic-RGD-PLGC(Me)AG-MMAE-ACPP and cyclic-RAD-PEG6-MMAE-ACPP peptides were diluted to 5 μmol/L in serum-free imaging buffer. The cells were treated with peptide for 25 minutes at 37°C and washed 3× before 100 μL of imaging buffer containing 10% FBS and 20 μg/mL Hoechst 33342 (Life Technologies) was added. Live cell imaging was performed as previously described in Cellular uptake and confocal imaging.

Published OnlineFirst April 15, 2014; DOI: 10.1158/1535-7163.MCT-13-1067



### Therapeutic studies

To generate MDA-MB-231 tumors, athymic *nu/nu* mice were injected in the upper thoracic mammary fat pads with $7.5 \times 10^5$ cancer cells in Matrigel at a concentration of 4 mg/mL. The volume of tumor cell injections ranged from 30 to 40 μL. For Py230 tumors, $1 \times 10^6$ cells were injected into the mammary fat pads of albino C57Bl/6 mice in 10 to 20 μL of 4 mg/mL Matrigel, and tumors grew for approximately 5 weeks before therapy began. Volumes were monitored at regular intervals with calipers and the volume was calculated with the following equation: volume $= {}^1/_2$ (length)(width)$^2$. Tumors were allowed to grow to a volume between 50 and 80 mm$^3$ before therapeutic intervention. MMAE was formulated in a 3% DMSO saline solution and peptides were stored as lyophilized powders and suspended in deionized water just before injection. All therapeutic constructs were administered intravenously. Maleimidocaproyl-Val-Cit-PAB-MMAE was used to synthesize the cyclic-RGD-PLGC(Me)AG-MMAE ACPP for all therapy experiments with the Py230 model. This resulted in a 3-carbon difference in the linker, as presented in Supplementary Fig. S1C.

## Results

Dual-targeted imaging peptides were generated by conjugating cyclic-RGD to the inhibitory domain of the PLGC(Me)AG-ACPP and the far-red fluorescent dye, Cy5, to the CPP domain. To evaluate the individual contributions of integrin binding and MMP activation, a variety of control peptides were also synthesized and tested. Dual-targeted peptides were generated that either controlled for integrin binding by replacing the cyclic-RGD motif with a cyclic-RAD or made impervious to enzymatic cleavage by substituting an uncleavable PEG6 linker for PLGC(Me)AG. All of the peptides used in this study, as well as synthetic intermediates, are presented in Supplementary Table S1 with detailed chemical structures presented in Supplementary Fig. S1.

To determine whether the addition of cyclic-RGD to the ACPP impacted the digestion of the substrate sequence by MMP-2, cleavage rates were compared for a panel of peptides. PLGC(Me)AG-ACPP, cyclic-RGD-PLGC(Me)AG-ACPP, cyclic-RAD-PLGC(Me)AG-ACPP, and cyclic-RGD-PEG6-ACPP were incubated with the catalytic domain of MMP-2 at 37°C and aliquots were taken at multiple time points for up to 4 hours. Cleavage was monitored by gel electrophoresis (Supplementary Fig. S2), and fluorescence intensity measurements of the bands were used to generate a plot of peptide hydrolysis over time (Fig. 2A). The addition of cyclic-RGD proximal to the ACPP substrate resulted in a slight reduction in cleavage rates at early time points. Substituting the cyclic-RGD with cyclic-RAD, a common control to eliminate integrin $\alpha_v\beta_3$ binding, had no impact on kinetics and the uncleavable peptide was resistant to MMP-2 degradation at all time points.

The affinity of cyclic-RGD for $\alpha_v\beta_3$, either alone or in the context of an ACPP, was measured using a cell-based competitive binding assay. MDA-MB-435 cells, labeled with Calcein Green, were incubated with varying concentration of peptides before being transferred to vitronectin, a protein ligand for $\alpha_v\beta_3$, coated plates. The cells were allowed to bind before the plates were washed. Using fluorescence of Calcein Green as the readout, it was established that conjugation of PLGC(Me)AG-ACPP to cyclic-RGD had little effect on the affinity of cyclic-RGD for integrin $\alpha_v\beta_3$ (Fig. 2B). Furthermore, the MMP-cleavable ACPP without the cyclic-RGD motif had minimal effects on cell binding to vitronectin, even at high peptide concentrations.

To determine whether there was a combined effect from targeting both integrins and MMPs, peptide uptake was observed with U87MG glioblastoma cells *in vitro*. U87MGs were incubated with 1 μmol/L peptide in serum-free media for 30 minutes at 37°C, washed, and imaged with confocal microscopy. PLGC(Me)AG-ACPP had greater cell uptake than cyclic-RGD, whereas the co-targeted cyclic-RGD-PLGC(Me)AG-ACPP had the highest intracellular fluorescence (Fig. 2C). Substitution of cyclic-RAD for cyclic-RGD resulted in similar uptake to PLGC(Me)AG-ACPP. Cyclic-RGD-PEG6-ACPP also showed much less cellular uptake, and fluorescence was almost undetectable with the double-negative cyclic-RAD-PEG6-ACPP.

Dual targeting was tested *in vivo* with orthotopic MDA-MB-231 mammary tumors. Representative images presented in Fig. 3A show mice 6 hours after intravenous administration of Cy5-labeled peptide. Tumor contrast was obtained with the skin and tumors targeted simultaneously via integrin $\alpha_v\beta_3$ and MMP-2 were the brightest (Fig. 3B). The tumor to surrounding tissue contrast ratio for cyclic-RGD-PLGC(Me)AG-ACPP was $7.8 \pm 1.6$, superior to all the other peptides (cyclic-RAD-PLGC(Me)AG-ACPP: $3.9 \pm 0.8$, $P = 3.5 \times 10^{-4}$; cyclic-RGD-PEG6-ACPP: $4.9 \pm 0.8$, $P = 3.1 \times 10^{-3}$; cyclic-RAD-PEG6-ACPP: $3.9 \pm 1.6$, $P = 2.2 \times 10^{-3}$). Congruent with the *in vitro* testing, the double targeted ACPP also had the highest tumor uptake, with a standardized uptake value (SUV) of $0.81 \pm 0.20$, significantly higher than cyclic-RAD-PLGC(Me)AG-ACPP (SUV: $0.27 \pm 0.11$, $P = 1.6 \times 10^{-6}$), RGD-PEG6-ACPP (SUV: $0.34 \pm 0.14$, $P = 2.6 \times 10^{-5}$), and cyclic-RAD-PEG6-ACPP (SUV: $0.15 \pm 0.04$, $P = 1.1 \times 10^{-8}$). Uptake of the probe in the liver and kidneys was similar for all peptides, with liver SUVs averaging 3.5 and kidney SUVs of ~15 (Supplementary Fig. S3).

To further validate the contribution of cyclic-RGD in this dual targeting strategy, the cyclic-RGD-PLGC(Me)AG-ACPP was co-injected with a 50-fold excess of unlabeled cyclic-(RGDfK). The tumor SUV for these mice was $0.20 \pm 0.06$, comparable to cyclic-RAD-PLGC(Me)AG-ACPP uptake (Supplementary Fig. S4). Thus, the benefit of cyclic-RGD is saturable and specific. In addition, a similar dual targeting strategy was devised using folate instead of cyclic-RGD. The attachment of folate to the

Published OnlineFirst April 15, 2014; DOI: 10.1158/1535-7163.MCT-13-1067



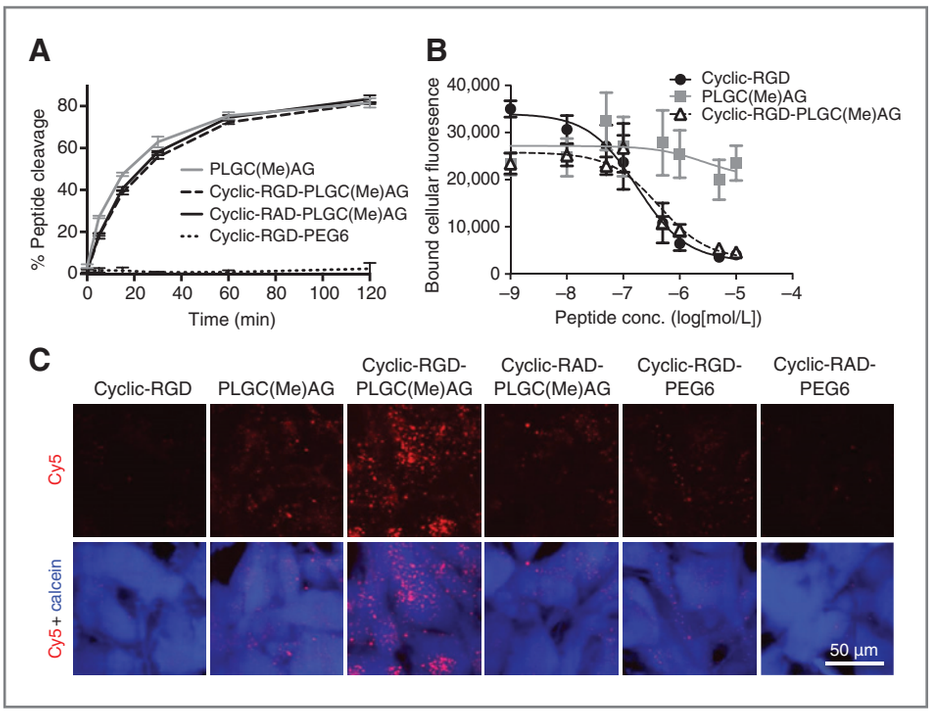


**Figure 2.** Combining cyclic-RGD and PLGC(Me)AG-ACPP does not impact activity or affinity while improving cellular uptake. A, about 5 μmol/L of Cy5-labeled peptide was incubated at 37°C with 50 nmol/L recombinant MMP-2. Samples at various time points were analyzed with gel electrophoresis, and enzyme cleavage was quantified using the intensities of the peptide bands. B, MDA-MB-435 cells were labeled with Calcein Green and incubated with 0 to 10 μmol/L peptide for 20 minutes at room temperature. Cells were transferred to vitronectin-coated plates and allowed to bind before any unadherent cells were gently removed. The peptide's ability to inhibit binding of integrins on the MDA-MB-435s to vitronectin was determined by measuring cellular fluorescence. C, U87MG glioblastoma cells were incubated with 1 μmol/L of Cy5-labeled peptide for 25 minutes at 37°C. Cells were washed, labeled with calcein blue, and imaged with confocal microscopy. Top row is peptide fluorescence (red), bottom row shows overlay of Cy5 fluorescence (red) and calcein blue (blue), a marker for cell viability.

MMP-cleavable ACPP had no impact on SKOV3 tumor uptake (Supplementary Fig. S5), an ovarian cancer model that expresses the folate receptor (25). Presumably, folate and the ACPP do not synergize because the folate receptor and MMP-2 do not form a molecular complex or reside in close proximity.

Having validated the cyclic-RGD dual-targeted peptide in the human MDA-MB-231 breast cancer model, further testing of cyclic-RGD-PLGC(Me)AG-ACPP was done in the context of a fully functional immune system. We used the polyomavirus middle T (PyMT) oncogene mouse model, which forms spontaneous mammary adenocarcinomas with metastatic potential (23), as well as the Py230 cell line that can be injected orthotopically to form syngeneic mammary tumors. The Py230 clonal cell line was derived from spontaneous PyMT tumor homogenates and has been characterized as generating luminal tumors when injected in mice (24). In both models, there was a clear identification of the tumor once the fur and skin was removed (Fig. 3C and D). The tumor contrast was $2.8 \pm 0.3$ for the PyMT model and $6.1 \pm 1.5$ for Py230. Finally, the ability of cyclic-RGD-PLGC(Me)AG-ACPP to detect pulmonary metastases was examined with an experimental lung metastasis model using Py230 cells. When looking at the whole lungs, metastatic lesions as small as 0.5 mm were detectable with approximately 2-fold contrast (Fig. 3E and F).

MDA-MB-231 tumors were sectioned to detect peptide distribution on a histologic level. Previously, it has been reported that free ACPPs cleavable by MMP-2/-9 home to the stromal regions of the tumor, without much penetration into the tumor tissue (6). With the addition of the cyclic-RGD motif, elevated Cy5 fluorescence was observed both around the perimeter of the tumor and throughout the tumor cross-section (Fig. 4A). With cyclic-RAD-PLGC(Me)AG-ACPP, the boundary of the tumor had the highest peptide signal. Conversion of PLGC(Me)AG to PEG6 substantially reduced fluorescence at the tumor margins, and almost no fluorescent signal was detected in tumor sections from mice that had been injected with cyclic-RAD-PEG6-ACPP. Peptide localization for cyclic-RGD-PLGC(Me)AG-ACPP was also visualized in MDA-MB-231 tumors *ex vivo* using confocal microscopy. Images of live tumor tissue revealed that the peptide was able to get beyond the vasculature and was primarily contained in endocytic vesicles within the cancer cells (Fig. 4B and C).

Immunohistochemistry was used to confirm the expression of both integrin $\alpha_v\beta_3$ and MMP-2 in MDA-MB-231 tumors, as well as to compare those expression patterns to

Published OnlineFirst April 15, 2014; DOI: 10.1158/1535-7163.MCT-13-1067



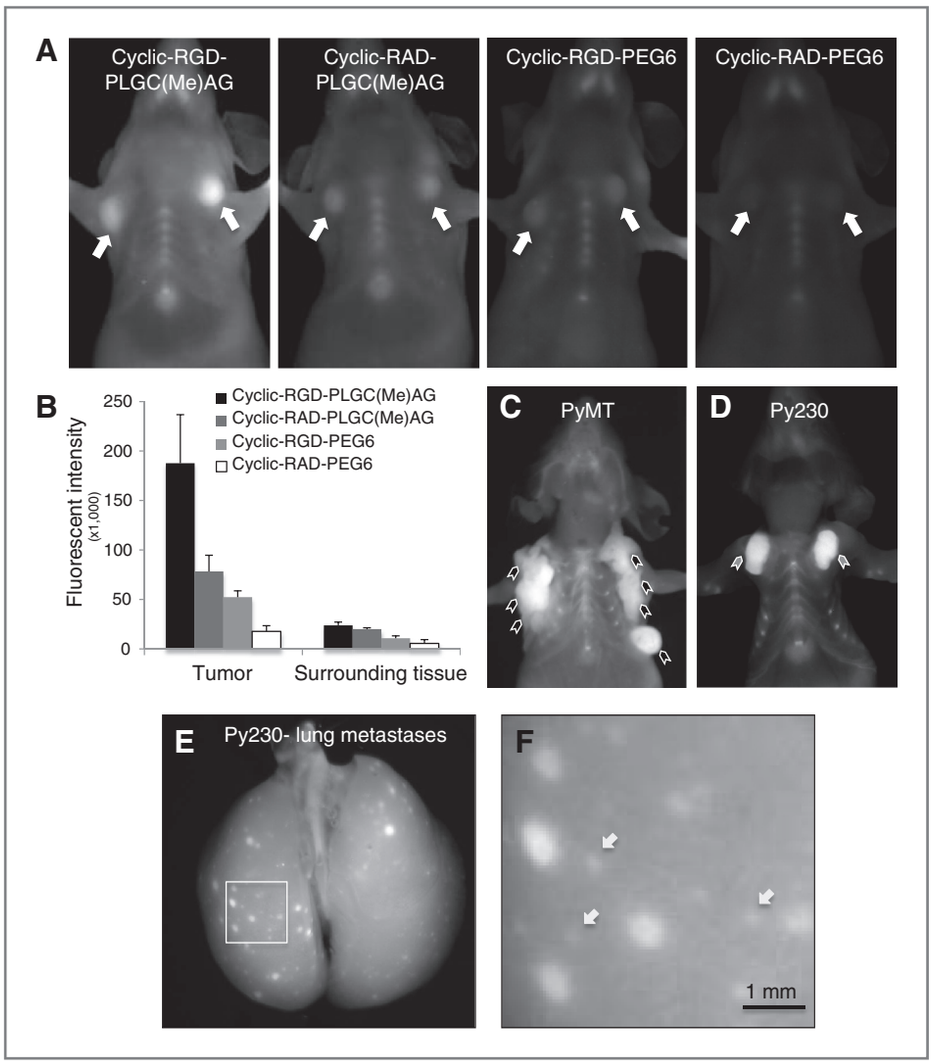


**Figure 3.** *In vivo* breast tumor imaging with dual-targeted ACPPs. A, dual-targeted cyclic-RGD-PLGC(Me)AG-ACPP, single-targeted (cyclic-RAD-PLGC(Me)AG-ACPP and cyclic-RGD-PEG6-ACPP), and double-negative cyclic-RAD-PEG6-ACPP peptides were injected into mice harboring bilateral orthotopic MDA-MB-231 breast cancer tumors. Six hours after a 10 nanomole dose, mice were anesthetized and imaged for Cy5 fluorescence. Tumors are indicated with white arrows. B, skin was removed and fluorescent intensities were measured for both the tumor and the surrounding tissue. C and D, cyclic-RGD-PLGC(Me)AG-ACPP was injected into mice with spontaneously forming polyomavirus (PyMT) mammary tumors, indicated with black arrowheads (C) or Py230 syngeneic orthotopic breast tumors, indicated with gray arrowheads (D). E, mice with Py230 lung metastases were injected with 10 nanomoles of cyclic-RGD-PLGC(Me)AG-ACPP and sacrificed 6 hours later. The trachea was exposed and the lungs were inflated with 800 μL aqueous PBS before imaging. F, higher magnification of the inlay shown in E. White arrows denote micrometastases that are visible with the cyclic-RGD-PLGC(Me)AG-ACPP.

that of cyclic-RGD-PLGC(Me)AG-ACPP labeling. Serial tumor sections were probed with fluorescent antibodies (Abs) against integrin $\alpha_v\beta_3$ or MMP-2, imaged for Cy5 signal, or stained with hematoxylin and eosin (H&E). When the fluorescent patterns are compared, it is clear that integrin $\alpha_v\beta_3$ and MMP-2 are in close proximity to one another and that cyclic-RGD-PLGC(Me)AG-ACPP localizes to regions of high target expression (Fig. 4). In the absence of a primary antibody, there was no fluorescence signal (Supplementary Fig. S6).

Next, the ability of the dual-targeted peptide to deliver a chemotherapeutic cargo was investigated. MMAE was attached to the polyarginine portion of the ACPP via a cathepsin B–cleavable linker. This linker is designed for degradation in the lysosome and upon cleavage, an unmodified MMAE is released, which is free to cross the vesicular membrane (26). First, cellular targeting for cyclic-RGD-PLGC(Me)AG-MMAE-ACPP and the control peptide, cyclic-RAD-PEG6-MMAE-ACPP, was tested in a variety of human cancer cell lines including breast, cervical, pancreatic, and prostate. The cells were incubated with peptide (5 μmol/L) for 25 minutes and washed before analysis using confocal microscopy. Cy5 fluorescence (red) established that the dual-targeted peptide had superior penetration in all cell lines compared with controls (Fig. 5).

For the *in vivo* studies, a therapeutic dose of 0.2 mg/kg MMAE (~6.5 nanomoles of the peptide–drug conjugate) was used. This dose was well under the maximum tolerated dose of 0.5 to 1.0 mg/kg (22, 27), and it correlates with a recent study targeting MMAE as a legumain activatable prodrug, which used free MMAE at 0.1 to 0.5 mg/kg (28). Tumor homing of the dual-targeted therapeutic peptides at the 6.5 nanomole dose was verified with fluorescence imaging (Fig. 6A). Tumor contrast through the skin was lower than previously seen with the imaging dose of 10 nanomoles, but cyclic-RGD-PLGC(Me)AG-MMAE-ACPP and cyclic-RGD-PLGC(Me)AG-ACPP had equivalent tumor

Published OnlineFirst April 15, 2014; DOI: 10.1158/1535-7163.MCT-13-1067



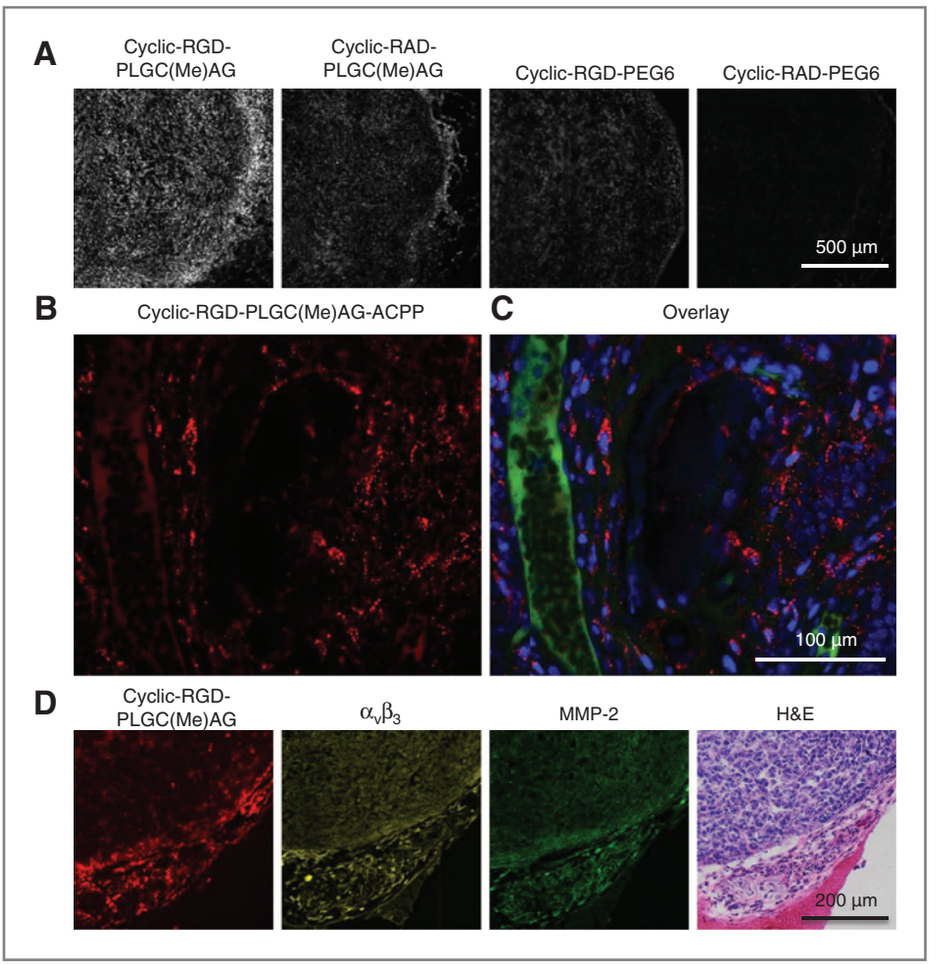


**Figure 4.** Intratumoral localization of dual-targeted peptides. A, Cy5-labeled ACPPs were injected into mice, and 6 hours later, MDA-MB-231 tumors were harvested and frozen in liquid nitrogen. Tumors were sectioned, mounted on slides, and then imaged using confocal microscopy. B and C, confocal imaging of MDA-MB-231 mammary tumors harvested 6 hours after being treated with 10 nanomoles cyclic-RGD-PLGC(Me)AG-ACPP. The mice were also dosed with FITC-dextran to visualize blood vessels and Hoechst, a nuclear stain, before tumor excision. Cy5 fluorescence is shown in B, and an overlay of Cy5 (red), FITC-dextran (green), and Hoechst (blue) is provided in C. D, cyclic-RGD-PLGC(Me)AG-ACPP peptide colocalizes with integrin $\alpha_v\beta_3$ and MMP-2 expression. Serial tumor sections were either imaged for Cy5 fluorescence (red) or probed with antibodies against integrin $\alpha_v\beta_3$ (yellow) and MMP-2 (green). A representative H&E is given in the last panel.

uptake that was superior to cyclic-RAD-PEG6-MMAE-ACPP, which showed no tumor contrast. The stability of cyclic-RGD-PLGC(Me)AG-MMAE-ACPP was tested in fresh mouse plasma, and the peptide remained intact after a 2-hour incubation enabling *in vivo* testing, as the peptide is more than 90% cleared from the blood 30 minutes postinjection (Supplementary Fig. S7).

MDA-MB-231 tumors were implanted into the mammary fat pads of female mice, and therapeutic intervention was initiated once the tumors reached the approximate volume of 50 $mm^3$. Seven mice per treatment group were randomly assigned to receive either no treatment, MMAE free drug, cyclic-RAD-PEG6-MMAE-ACPP, or cyclic-RGD-PLGC(Me)AG-MMAE-ACPP at a dose of 0.2 mg/kg MMAE. The drugs were administered every 3 days for a total of 4 doses. Cyclic-RGD-PLGC(Me)AG-ACPP targeting of MMAE significantly ($P = 3.1 \times 10^{-3}$) reduced the average tumor volume over treatment with the drug alone (Supplementary Fig. S8A). When the targeting mechanisms were controlled for using a cyclic-RAD-PEG6-ACPP, it was substantially less effective than equimolar free MMAE. Once tumors grew to a diameter of 10 mm, the animals were sacrificed, so experimental analysis continued by monitoring survival of the remaining animals. The data are presented as a Kaplan–Meier survival plot that begins after the last therapy injection (Fig. 6B). Conjugating MMAE with cyclic-RGD-PLGC(Me)AG-ACPP prolonged animal survival, with 28% of the mice in this treatment group attaining complete tumor regression. All animals treated with either MMAE or cyclic-RAD-PEG6-MMAE-ACPP had to be sacrificed by 19 days posttherapy.

To determine the contribution of each targeting moiety to the therapeutic effect, cyclic-RAD-PLGC(Me)AG-MMAE-ACPP and cyclic-RGD-PEG6-MMAE-ACPP were synthesized and tested to eliminate one mechanism at a time. This extended panel of peptides was administered to mice bearing MDA-MB-231 tumors at a dose of 0.22 mg/kg MMAE (~7 nmole dose) as indicated by the black arrows in Fig. 6C. Again, the dual-targeted peptide significantly reduced tumor volume when compared with the drug alone ($P = 2.0 \times 10^{-3}$) and achieved tumor regression in 1 of 4 mice. When each targeting strategy was tested individually, the result was similar to that of the dual negative probe; peptide conjugation reduced the

Published OnlineFirst April 15, 2014; DOI: 10.1158/1535-7163.MCT-13-1067



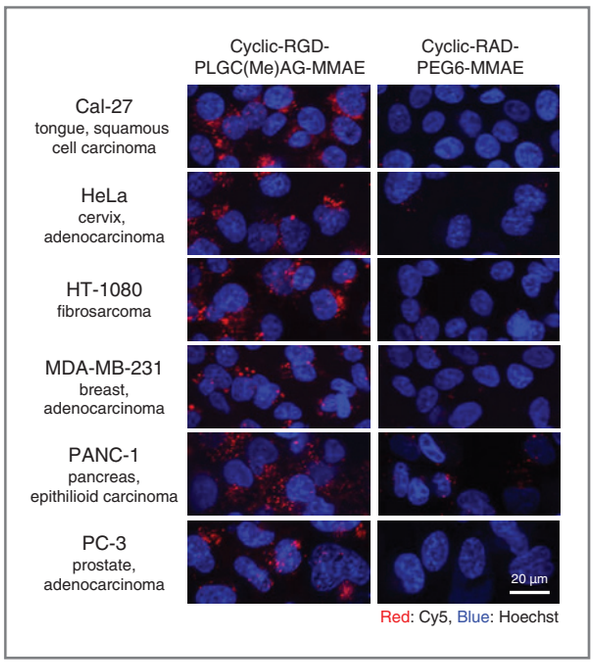


**Figure 5.** Cyclic-RGD-PLGC(Me)AG-MMAE-ACPP is preferentially taken up into a variety of human cancer cell lines *in vitro*. Cyclic-RGD-PLGC(Me)AG-MMAE-ACPP (left column) and cyclic-RAD-PEG6-MMAE-ACPP (right column) were incubated on several human cancer cell lines at 5 μmol/L in serum-free media at 37°C for 25 minutes. The cells were washed and then imaged live using a 5-Live confocal microscope. Cy5 fluorescence (red) for the 2 peptides is scaled equally within each cell line, and across cell lines, the cyclic-RGD-PLGC(Me)AG-MMAE-ACPP signal is scaled to max. The nuclei were labeled with Hoechst nuclear stain, which is represented in blue.

efficacy of MMAE. Animal body weights remained constant for all treatment groups, suggesting no overt toxicity as a result of therapy (Supplementary Fig. S8B). When the dose of cyclic-RGD-PLGC(Me)AG-MMAE-ACPP was increased to 40 nanomoles (equivalent to 1.2 mg/kg MMAE), animals began to lose weight after the first injection and had to be sacrificed before any therapeutic affect could be observed (Supplementary Fig. S9). When the dose was halved to 20 nanomoles (equivalent to 0.6 mg/kg MMAE), animals maintained their initial weights and had near-complete tumor regression.

Dual targeting was then tested in the Py230 tumor model and compared with MMAE alone. The first experiment was done at a dose similar to MDA-MB-231, but in this immunocompetent model, 0.2 mg/kg of MMAE had no impact on tumor growth whereas the cyclic-RGD-PLGC(Me)AG-MMAE-ACPP reduced tumor volume by 40% compared to the controls, $P = 0.09$ (Supplementary Fig. S10). Mice bearing Py230 tumors were then treated with MMAE at concentrations up to 0.6 mg/kg to determine what dose resulted in a therapeutic response. Only the tumors treated at the highest dose had a reduction in final mass and none of the animals demonstrated weight loss (Supplementary Fig. S10B and S10C). Dual targeting was tested again, at a dose of 0.5 mg/kg MMAE. Free drug did not stop Py230 tumor growth, whereas cyclic-RGD-PLGC(Me)AG-MMAE-ACPP was completely able to inhibit the growth ($P < 0.01$, Fig. 6D).

## Discussion

The combination of integrin and MMP targeting was successful at amplifying tumor targeting beyond levels attained by either mechanism alone. The attachment of cyclic-RGD near the substrate region of the ACPP had a minimal effect on MMP-2 cleavage rates and did not impact the affinity of cyclic-RGD for integrin $\alpha_v\beta_3$. While it is clear from cell culture experiments that dual targeting has a supra additive effect on peptide uptake, it would be interesting to monitor peptide cleavage kinetics in a similar biologic context. One report designed a MMP-RGD peptide that released fluorescein (FAM) into the culture media upon cleavage by MMP-2 (29). This article shows no difference in peptide cleavage when incubating the probe on PMA-treated HUVEC cells with or without a 10-fold excess of cyclic-RGD. In this experiment, no cleavage of their probe was detected in the first 8 hours of incubation, and it was not until 24 hours postinjection that an increase in the concentration of released FAM was measured. At this time point, active MMP-2 was found in the culture media, suggesting that cleavage could be a result of unbound MMP-2, so the lack of integrin dependence is not surprising. Also, the time scale for these experiments is drastically different from that observed with cyclic-RGD-PLGC(Me)AG-ACPP in tissue culture, which after washing off any soluble enzyme, had a substantial increase in peptide cleavage and cellular uptake within 20 minutes.

*In vivo* results also support the hypothesis that dual targeting with cyclic-RGD and MMP-2 cleavable ACPPs improves tumor targeting. Systematic controls for integrin binding and MMP-2 susceptibility clearly demonstrated that combining both targeting moieties resulted in superior peptide uptake and improved contrast to surrounding tissues. Imaging peptide fluorescence on a histologic scale supported the gross fluorescent data. Cross-sections of tumors from mice that had been injected with cyclic-RGD-PLGC(Me)AG-ACPP had substantially more peptide fluorescence with labeling distributed throughout the tumor. With just MMP targeting, the fluorescence was localized to the tumor edges, and once the enzymatic targeting was disabled, tumor signal dropped dramatically. Further support for the functional relationship between integrin $\alpha_v\beta_3$ and MMP-2 comes from the data obtained with the folate-PLGC(Me)AG-ACPP peptide. There is no known association between MMP-2 and the folate receptor and subsequently, the attachment of folate to the ACPP yielded no increase in tumor fluorescence or uptake when tested in an ovarian cancer model known to express the folate receptor.

The results in the MDA-MB-231 tumor model are particularly exciting because of this cell line's triple-negative

Published OnlineFirst April 15, 2014; DOI: 10.1158/1535-7163.MCT-13-1067



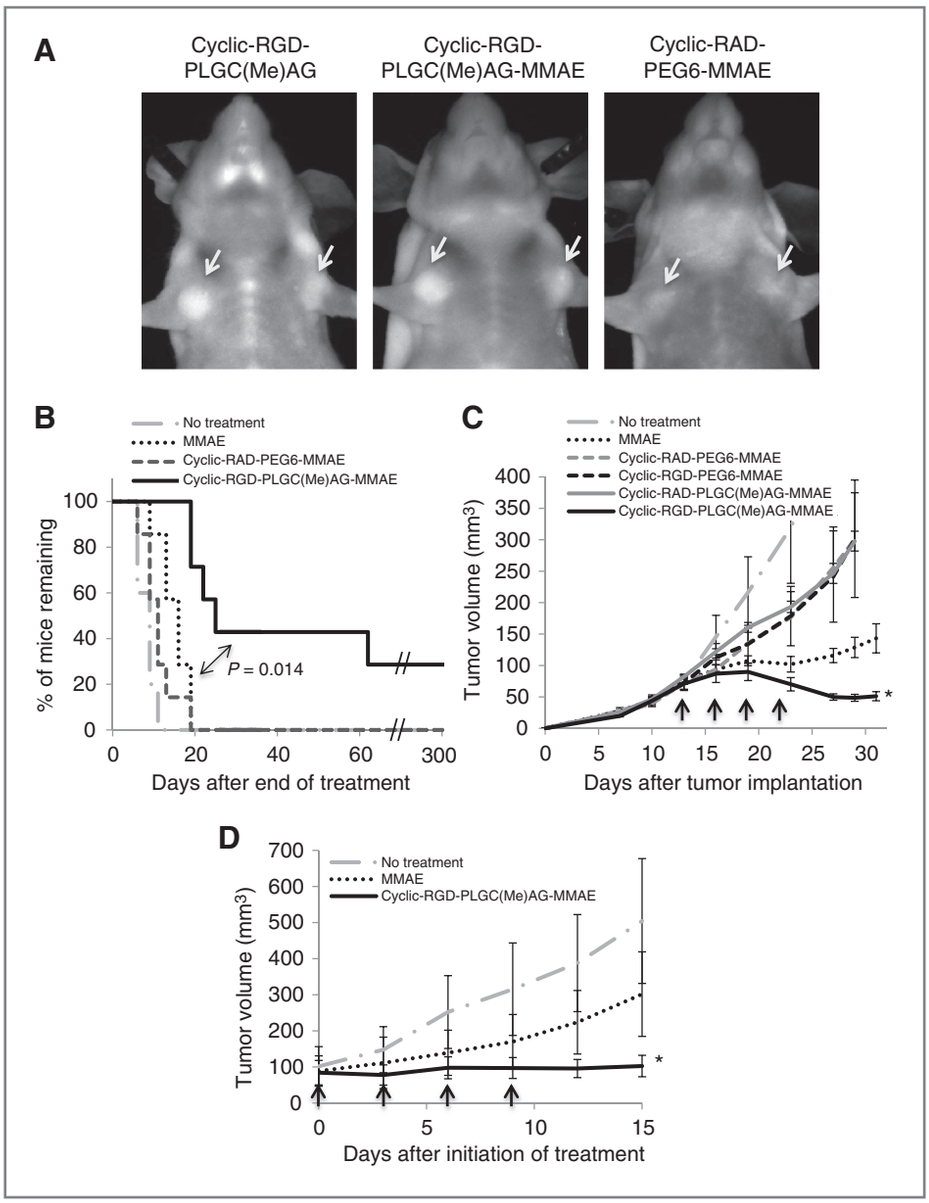


**Figure 6.** Targeting of MMAE with cyclic-RGD-PLGC(Me)AG-ACPP significantly improved therapeutic efficacy in human and syngeneic breast cancer models. A, mice with MDA-MB-231 tumors (~5 mm in diameter) were injected with 6.5 nanomoles of Cy5-labeled peptides as indicated. Six hours postinjection, animals were anesthetized and imaged for Cy5 fluorescence. White arrows denote the location of the mammary tumors. B, mice with MDA-MB-231 tumors in both the left and right mammary fat pads (~50 $mm^3$) were divided into treatments groups ($n = 7$) and received no treatment, MMAE alone, cyclic-RGD-PLGC(Me)AG-MMAE-ACPP, or cyclic-RAD-PEG6-MMAE-ACPP. The MMAE dose for each therapeutic agent is equivalent to 0.2 mg/kg. Treatment was administered every 3 days for a total of 4 doses, and a Kaplan–Meier curve was generated beginning on the last day of therapeutic intervention. Animals were sacrificed once a tumor grew to a diameter of ≥10 mm. Statistical analysis was performed using SigmaPlot's log-rank survival statistics. C, mice with MDA-MB-231 tumors ($n = 4$) received no treatment, MMAE alone, cyclic-RGD-PLGC(Me)AG-MMAE-ACPP, cyclic-RAD-PLGC(Me)AG-MMAE-ACPP, cyclic-RGD-PEG6-MMAE-ACPP, or cyclic-RAD-PEG6-MMAE-ACPP at a dose equivalent to 0.22 mg/kg MMAE (~7 nanomoles of peptide). Mice were treated as indicated by black arrows. D, immunocompetent mice ($n = 4$) harboring syngeneic Py230 tumors (~80 $mm^3$) were administered MMAE or cyclic-RGD-PLGC(Me)AG-MMAE-ACPP at a dose of 0.5 mg/kg (~16 nanomoles) as denoted by the black arrows. *, $P < 0.01$ (Student $t$ test) for MMAE versus cyclic-RGD-PLGC(Me)AG-MMAE-ACPP.

status; these cells do not rely on the overexpression of estrogen, progesterone, or HER2 receptors (30). Patients with triple-negative tumors have bad prognoses (31) and they do not benefit from current molecularly targeted therapies such as trastuzumab and tamoxifen. Development of targeting agents like ACPPs, which use the ubiquitous expression of gelatinases in tumor progression and malignancy, could provide an exciting new avenue for

Published OnlineFirst April 15, 2014; DOI: 10.1158/1535-7163.MCT-13-1067



therapeutic development for multiple types of cancer. This is supported by the fact that dual-targeted ACPPs had superior tumor cell uptake across multiple human cancer cell types.

A recent report also uses dual targeting to deliver MMAE by combining legumain protease activation and integrin targeting (32). This article focuses on how the prodrug formulation of MMAE increases its therapeutic window, showing a reduction in primary tumor volume and metastatic burden using 3 times the maximum tolerated dose of MMAE alone. The therapy experiments do not have controls to validate the proposed mechanism and primarily compare animal data for prodrug-MMAE with mice that are not receiving treatment. Our dual-targeted ACPPs are demonstrating similar therapeutic results as those reported in Lui and colleagues but at a fraction (7%) of the dose. This is promising evidence that dual-targeted ACPPs can be a powerful tool to for the intracellular delivery of diagnostic and therapeutic agents to the regions of enzymatic activity associated with tumor progression.

## Disclosure of Potential Conflicts of Interest

R.Y. Tsien has ownership interest (including patents) in and is a consultant/advisory board member for Avelas Biosciences. M.A. Whitney is a consultant/advisory board member for Avelas Biosciences. No potential conflicts of interest were disclosed by the other authors.

## Authors' Contributions

**Conception and design:** J.L. Crisp, E.N. Savariar, M.A. Whitney, R.Y. Tsien
**Development of methodology:** J.L. Crisp, E.N. Savariar, M.A. Whitney, R.Y. Tsien
**Acquisition of data (provided animals, acquired and managed patients, provided facilities, etc.):** J.L. Crisp, E.N. Savariar, H.L. Glasgow, L.G. Ellies
**Analysis and interpretation of data (e.g., statistical analysis, biostatistics, computational analysis):** J.L. Crisp, E.N. Savariar, H.L. Glasgow, M.A. Whitney
**Writing, review, and/or revision of the manuscript:** J.L. Crisp, E.N. Savariar, M.A. Whitney, R.Y. Tsien
**Study supervision:** M.A. Whitney, R.Y. Tsien

## Acknowledgments

The authors thank Dr. Peter Senter for invaluable discussion, Paul Steinbach for assistance with confocal microscopy, Qing Xiong for support with solid phase peptide synthesis, and Perla Arcaira for her support with animal husbandry and tumor model generation.

## Grant Support

This work was supported by the Howard Hughes Medical Institute (to R.Y. Tsien), the NIH/NCI grant 5R01CA158448 (to E.N. Savariar, L.G. Ellies, M.A. Whitney, and R.Y. Tsien), and the DoD Breast Cancer Collaborative Innovators Award W81XWH-09-1-0699 (to J.L. Crisp, H.L. Glasgow, and R.Y. Tsien).

The costs of publication of this article were defrayed in part by the payment of page charges. This article must therefore be hereby marked *advertisement* in accordance with 18 U.S.C. Section 1734 solely to indicate this fact.

Received December 17, 2013; revised March 24, 2014; accepted April 9, 2014; published OnlineFirst April 15, 2014.

## References

1. Jiang T, Olson ES, Nguyen QT, Roy M, Jennings PA, Tsien RY. Tumor imaging by means of proteolytic activation of cell-penetrating peptides. Proc Natl Acad Sci U S A 2004;101:17867–72.
2. Chambers AF, Matrisian LM. Changing views of the role of matrix metalloproteinases in metastasis. J Natl Cancer Inst 1997;89:1260–70.
3. Overall CM, Kleifeld O. Tumour microenvironment - opinion: validating matrix metalloproteinases as drug targets and anti-targets for cancer therapy. Nat Rev Cancer 2006;6:227–39.
4. Talvensaari-Mattila A, Paakko P, Turpeenniemi-Hujanen T. Matrix metalloproteinase-2 (MMP-2) is associated with survival in breast carcinoma. Br J Cancer 2003;89:1270–5.
5. Nguyen QT, Olson ES, Aguilera TA, Jiang T, Scadeng M, Ellies LG, et al. Surgery with molecular fluorescence imaging using activatable cell-penetrating peptides decreases residual cancer and improves survival. Proc Natl Acad Sci U S A 2010;107:4317–22.
6. Olson ES, Aguilera TA, Jiang T, Ellies LG, Nguyen QT, Wong EH, et al. *In vivo* characterization of activatable cell penetrating peptides for targeting protease activity in cancer. Integr Biol 2009;1:382–93.
7. Olson ES, Jiang T, Aguilera TA, Nguyen QT, Ellies LG, Scadeng M, et al. Activatable cell penetrating peptides linked to nanoparticles as dual probes for *in vivo* fluorescence and MR imaging of proteases. Proc Natl Acad Sci U S A 2010;107:4311–6.
8. Brooks PC, Stromblad S, Sanders LC, von Schalscha TL, Aimes RT, Stetler-Stevenson WG, et al. Localization of matrix metalloproteinase MMP-2 to the surface of invasive cells by interaction with integrin alpha v beta 3. Cell 1996;85:683–93.
9. Brooks PC, Clark RA, Cheresh DA. Requirement of vascular integrin alpha v beta 3 for angiogenesis. Science 1994;264:569–71.
10. Hood JD, Cheresh DA. Role of integrins in cell invasion and migration. Nat Rev Cancer 2002;2:91–100.
11. Ruoslahti E. Specialization of tumour vasculature. Nat Rev Cancer 2002;2:83–90.
12. Jiao Y, Feng X, Zhan Y, Wang R, Zheng S, Liu W, et al. Matrix metalloproteinase-2 promotes alphavbeta3 integrin-mediated adhesion and migration of human melanoma cells by cleaving fibronectin. PLoS ONE 2012;7:e41591.
13. Deryugina EI, Ratnikov B, Monosov E, Postnova TI, DiScipio R, Smith JW, et al. MT1-MMP initiates activation of pro-MMP-2 and integrin alphavbeta3 promotes maturation of MMP-2 in breast carcinoma cells. Exp Cell Res 2001;263:209–23.
14. Puyraimond A, Fridman R, Lemesle M, Arbeille B, Menashi S. MMP-2 colocalizes with caveolae on the surface of endothelial cells. Exp Cell Res 2001;262:28–36.
15. Mebrahtu E, Zheleznyak A, Hur MA, Laforest R, Lapi SE. Initial characterization of a dually radiolabeled peptide for simultaneous monitoring of protein targets and enzymatic activity. Nucl Med Biol 2013;40:190–6.
16. Zhu L, Xie J, Swierczewska M, Zhang F, Lin X, Fang X, et al. Dual-functional, receptor-targeted fluorogenic probe for *in vivo* imaging of extracellular protease expressions. Bioconjug Chem 2011;22:1001–5.
17. Pettit GR. The dolastatins. Fortschr Chem Org Naturst 1997;70:1–79.
18. Mohammad RM, Limvarapuss C, Wall NR, Hamdy N, Beck FW, Pettit GR, et al. A new tubulin polymerization inhibitor, auristatin PE, induces tumor regression in a human Waldenstrom's macroglobulinemia xenograft model. Int J Oncol 1999;15:367–72.
19. Senter PD, Sievers EL. The discovery and development of brentuximab vedotin for use in relapsed Hodgkin lymphoma and systemic anaplastic large cell lymphoma. Nat Biotechnol 2012;30:631–7.
20. Okeley NM, Alley SC, Senter PD. Advancing antibody drug conjugation: from the laboratory to a clinically approved anticancer drug. Hematol Oncol Clin North Am 2014;28:13–25.
21. Savariar EN, Felsen CN, Nashi N, Jiang T, Ellies LG, Steinbach P, et al. Real-time *in vivo* molecular detection of primary tumors and metastases with ratiometric activatable cell-penetrating peptides. Cancer Res 2013;73:855–64.

Published OnlineFirst April 15, 2014; DOI: 10.1158/1535-7163.MCT-13-1067




22. Francisco JA, Cerveny CG, Meyer DL, Mixan BJ, Klussman K, Chace DF, et al. cAC10-vcMMAE, an anti-CD30-monomethyl auristatin E conjugate with potent and selective antitumor activity. Blood 2003;102:1458–65.
23. Guy CT, Cardiff RD, Muller WJ. Induction of mammary tumors by expression of polyomavirus middle T oncogene: a transgenic mouse model for metastatic disease. Mol Cell Biol 1992;12:954–61.
24. Gibby K, You WK, Kadoya K, Helgadottir H, Young LJ, Ellies LG, et al. Early vascular deficits are correlated with delayed mammary tumorigenesis in the MMTV-PyMT transgenic mouse following genetic ablation of the NG2 proteoglycan. Breast Cancer Res 2012;14:R67.
25. Miotti S, Bagnoli M, Ottone F, Tomassetti A, Colnaghi MI, Canevari S. Simultaneous activity of two different mechanisms of folate transport in ovarian carcinoma cell lines. J Cell Biochem 1997;65:479–91.
26. Dubowchik GM, Firestone RA. Cathepsin B-sensitive dipeptide prodrugs. 1. A model study of structural requirements for efficient release of doxorubicin. Bioorg Med Chem Lett 1998;8:3341–6.
27. Mirsalis JC, Schindler-Horvat J, Hill JR, Tomaszewski JE, Donohue SJ, Tyson CA. Toxicity of dolastatin 10 in mice, rats and dogs and its clinical relevance. Cancer Chemother Pharmacol 1999;44:395–402.
28. Bajjuri KM, Liu Y, Liu C, Sinha SC. The legumain protease-activated auristatin prodrugs suppress tumor growth and metastasis without toxicity. ChemMedChem 2011;6:54–9.
29. Vartak DG, Lee BS, Gemeinhart RA. *In vitro* evaluation of functional interaction of integrin alphavbeta3 and matrix metalloprotease-2. Mol Pharm 2009;6:1856–67.
30. Chavez KJ, Garimella SV, Lipkowitz S. Triple negative breast cancer cell lines: one tool in the search for better treatment of triple negative breast cancer. Breast Dis 2010;32:35–48.
31. van 't Veer LJ, Dai H, van de Vijver MJ, He YD, Hart AA, Mao M, et al. Gene expression profiling predicts clinical outcome of breast cancer. Nature 2002;415:530–6.
32. Liu Y, Bajjuri KM, Liu C, Sinha SC. Targeting cell surface alpha(v)beta(3) integrin increases therapeutic efficacies of a legumain protease-activated auristatin prodrug. Mol Pharm 2012;9:168–75.

Published OnlineFirst April 15, 2014; DOI: 10.1158/1535-7163.MCT-13-1067

Molecular Cancer Therapeutics

# Dual Targeting of Integrin $\alpha_v\beta_3$ and Matrix Metalloproteinase-2 for Optical Imaging of Tumors and Chemotherapeutic Delivery

Jessica L. Crisp, Elamprakash N. Savariar, Heather L. Glasgow, et al.

*Mol Cancer Ther* 2014;13:1514-1525. Published OnlineFirst April 15, 2014.